

Electron temperature of hot spots in quantum Hall conductors

S. Komiyama, H. Sakuma, and K. Ikushima

Department of Basic Science, University of Tokyo, Komaba 3-8-1, Meguro-ku, Tokyo 153-8902, Japan

K. Hirakawa

Institute of Industrial Science, University of Tokyo, Komaba, Meguro-ku, Tokyo 153-8505, Japan

(Received 27 July 2005; revised manuscript received 7 December 2005; published 31 January 2006)

Spectroscopic studies are carried out on the cyclotron emission from the hot spots of GaAs/AlGaAs two-dimensional electron gas systems in a quantum Hall regime at $B=6.0$ T ($\nu=2.5$) and 7.5 T ($\nu=2.0$) at $T=4.2$ K by applying a terahertz scanning microscope. The spectra at the current entry and exit corners (hot spots) are remarkably broadened towards lower frequencies with increasing I up to $300 \mu\text{A}$, indicating the significant relevance of higher excited Landau levels. The spectra are analyzed by assuming that the effective electron temperature, T_E , at the local injection/withdrawal point reaches a maximum ~ 300 K while it is $T_E=25\text{--}30$ K when averaged over the region determined by the spatial resolution ($50 \mu\text{m}$ diameter).

DOI: [10.1103/PhysRevB.73.045333](https://doi.org/10.1103/PhysRevB.73.045333)

PACS number(s): 73.43.-f

The quantum Hall (QE) effect of two-dimensional gas (2DEG) systems in high magnetic fields provides a nontrivial problem in true physical conductors; that is, transferring electrons across the interface between a dissipationless 2DEG layer and dissipative metallic contacts. The problem is a prototype for mesoscopic conductors, in which electrical resistance is determined by elastic scattering processes inside the conductor while the energy dissipation takes place outside the conductor. When a current is passed through a quantum Hall (QH) bar, a voltage drop occurs locally at the diagonally opposite corners of the interfaces, at which electrons enter and leave the dissipation-less 2DEG layer.¹ These corners, called hot spots, are the locations where the total power is dissipated. Experimentally, excellent quantization of two-terminal resistance has been established, indicating the absence of excess contact resistance at the interface.² This suggested that tunneling process is essential and that the physical region through which electrons enter or leave the 2DEG layer is well localized in a microscopic region. Since the voltage drop at the hot spots can reach an order of 1 V in typical experimental conditions, the tunneling process must lead to significant generation of highly energetic electrons.

Several experimental attempts have been made to study the kinetics of electrons at the hot spots,^{3–10} with underlying interest in its possible influence on the quantization of resistance¹¹ or on the breakdown of the QH effect.^{9,12} Interest about the dynamics of the entry (exit) of electrons has led to theoretical considerations.^{8,13–15} Particularly, a consistent model supported by experiments^{2,8–11,16} has been obtained in Ref. 8. Spatial distribution of nonequilibrium electrons around the hot spots has recently been revealed by imaging cyclotron radiation, or the cyclotron emission (CE), from nonequilibrium electrons.^{8–10} Despite all those previous studies, however, the key issue of the hot spot, or the energy distribution of the nonequilibrium electrons, has been left completely unknown because of experimental difficulties.

Here, we carry out spectroscopic studies of spatially resolved CE to gain information about the energy distribution of nonequilibrium electrons. By applying a novel terahertz (THz) microscope, we find that CE spectra at the hot spots

are significantly distorted with substantial broadening towards lower frequencies. Noting a conduction band nonparabolicity in GaAs,^{17,18} we argue that electrons are significantly distributed in higher Landau levels (LLs) up to $N=4$, while the Fermi level lies in $N=1$ LL or in the gap region between $N=0$ and $N=1$ LLs. We suggest that at the lattice temperature of 4.2 K the effective electron temperature, T_E , reaches as high as $T_E \approx 300$ K at the spot center while it decreases rapidly as the location moves away from the spot, yielding an averaged value of $T_E=25\text{--}30$ K over the focal area under study ($50 \mu\text{m}$).

The CEs studied in this work are below a subpicowatt level. Resolving spectra of such weak THz radiations are nontrivial. We use a novel highly-sensitive scanning THz microscope shown in Fig. 1, which has been developed based on the earlier microscope (spatial resolution: $50 \mu\text{m}$).¹⁹ As described elsewhere in detail,²⁰ the wavelength is resolved (spectral resolution: $\Gamma_d=1.2 \text{ cm}^{-1}$) by magnetically tuning a quantum-Hall detector.

The samples are fabricated in a GaAs/Al_xGa_{1-x}As heterostructure crystal with an electron density and a mobility of $n_s=3.7 \times 10^{15}/\text{m}^2$ and $\mu=60 \text{ m}^2/\text{V s}$, respectively, at $T=4.2$ K. The samples are shaped into 3-mm-long and 0.5-mm-wide Hall bars, as outlined by broken lines in the upper panel of Fig. 2(a). Electrodes 1 and 5 serve as the source and the drain contacts. All the experiments are made at 4.2 K. The studies are made in the $\nu=2.0$ QH state ($B=7.52$ T) and $\nu=2.5$ state ($B=6.02$ T). The CE spectra at the hot spots are similar between $\nu=2.0$ and $\nu=2.5$, but CE along the edge of the sample is visible only at $\nu=2.5$.²¹ To utilize the CE along the edge as reference, we present here the data at $B=6.02$ T.

The topmost panel of Fig. 2 displays a two-dimensional (2D) image of CE taken with $I=50 \mu\text{A}$, where strong CE is seen around the two diagonally opposite corners (hot spots) and weaker CE along the edge of the lower potential boundary. The relative emission intensity per unit area is, roughly, 50:40:1 ($I=50 \mu\text{A}$) for the source hot spot (– electrode), the drain hot spot (+ electrode) and the edge region. In absolute

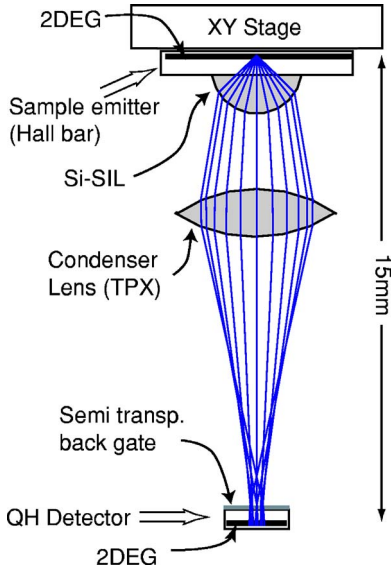


FIG. 1. (Color online) The scanning THz microscope. The quantum Hall device to be studied is mounted on an XY stage and is moved with respect to the solid immersion lens (SIL) made of Si. The electron density of the detector is controlled by the semi-transparent back gate.

terms, the CE in the edge region is on the order of several tens of femtowatts (from an area of $50 \mu\text{m}$ diameter). The area of CE around the hot spot spreads beyond the resolution limit ($50 \mu\text{m}$) as seen in the expanded 2D image and by the profiles displayed in the upper panel of Fig. 2. For the study of hot spots, the focal point of the microscope is placed at the location of maximum intensity.

The emission spectra in respective regions are compared in Figs. 2(a) and 2(b) for $I=50$ and $300 \mu\text{A}$, respectively, where the peak height of each line is normalized. The emission intensity at the hot spots for $I=300 \mu\text{A}$ is by a factor about 3 higher than that for $I=50 \mu\text{A}$. The spectra in the edge region are relatively narrow, symmetric, and kept substantially unchanged with increasing I from 50 to $300 \mu\text{A}$. Both spectra are well described by the Lorentzian curve, $1/[(\omega-\omega_0)^2+(\Gamma/2)^2]$, with $\omega_0=80.5 \text{ cm}^{-1}$ and $\Gamma=4.35 \text{ cm}^{-1}$ as shown by the solid lines in Figs. 2(a) and 2(b). By contrast, the spectra in the hot spots are asymmetrically broadened towards lower frequencies whereas the peak position shifts only slightly. The asymmetric broadening is enhanced at $I=300 \mu\text{A}$. These features, similar between the source and the drain hot spots, definitely indicate that nonequilibrium electrons are excited in higher LLs.

We begin with brief discussion of the spectrum in the edge region. The peak frequency, $\omega_0=80.5 \text{ cm}^{-1}$ ($\hbar\omega_0=9.98 \text{ meV}$), corresponds to the cyclotron effective mass of $m_c^*=0.0698m_0$ (m_0 ; the free electron mass). This strongly suggests the transition from the first excited Landau level ($N=1$ LL) to the lowest LL ($N=0$). The symmetric Lorentzian spectrum rules out substantial relevance of higher excited LLs ($N\geq 2$). The true spectral width, $\Gamma_{CE}=\Gamma-\Gamma_d=3.15 \text{ cm}^{-1}$, is comparable to the linewidth of CR absorption lines reported for 2DEG layers with similar

values of μ , n_s , and ν .^{22,23} The irrelevance of higher-level transitions is also consistent with the underlying mechanism of nonequilibrium electron generation discussed in Ref. 21.

At the source hot spot the electron injection from the source reservoir to the 2DEG layer is known to take place via electron tunneling into higher LLs as schematically illustrated in Fig. 3(a).^{8,24} At the drain hot spot inter-LL tunneling, $N\rightarrow N+1$, takes place before electrons enter the drain reservoir as depicted in Fig. 3(b).⁸ Since the electrochemical potential difference between the source and the drain reservoirs, $\mu_s-\mu_d=eV_{SD}$, is by a factor more than 50 larger than $\hbar\omega_c$ when $I\geq 50 \mu\text{A}$, we expect that higher LLs up to $N\geq 50$ are fed with electrons via tunneling in either hot spot region. After the tunneling events, the energetic electrons will rapidly release their excess energies via cascadelike emission of optical phonons ($\hbar\omega_{op}=36 \text{ meV}$),^{25,26} until they eventually fall into the lower energy region, $E<E_1+\hbar\omega_{op}$ (E_1 is the energy of the first excited LL), where the optical phonon emission is no longer possible. Since the energy relaxation process switches to much slower acoustical phonon emission, significant electron distribution is expected only in the LLs with $N\leq 4$ at $B=6 \text{ T}$.

The LL energy spacing, $\Delta E_N=E_{N+1}-E_N$, is reduced for higher values of N due to the conduction band nonparabolicity.^{18,19,27} By taking into account the effects of 2DEG quantization and LL quantization, we can derive an approximate expression²⁸

$$\Delta E_N = \hbar\omega_c \left[1 - 2 \left(\frac{\hbar\omega_c}{E_g^*} \right) (N+1) + 2 \left(\frac{\hbar\omega_c}{E_g^*} \right)^2 (3N^2 + 6N + \frac{13}{4}) \right] \left[1 - \frac{e}{3E_g^*} \left(\frac{eh^2}{m^* \epsilon^2} \right)^{1/3} \left(n_d + \frac{1}{2} n_s \right)^{2/3} \right], \quad (1)$$

where $E_g^*=0.98 \text{ eV}$ is an effective energy gap of GaAs, $m_0^*=0.066m_0$ is the band edge mass, $\epsilon=11.91\epsilon_0$ the dielectric constant of GaAs, n_d is the residual donor density in the depletion layer, and $\hbar\omega_c=eB/m_0^*$. For the 2DEG layer studied ($n_s=3.7\times 10^{15}/\text{m}^2$, $n_d=3\times 10^{14}/\text{m}^2$, $B=6.02 \text{ T}$), Eq. (1) is reduced to a simple prediction that the CE frequency decreases by a step of 1.9% as N increases by 1.

We assume that the population of N th LLs ($N\leq 4$) is characterized by the Fermi distribution function $f_N=1/\{1+\exp[(E_N-\mu)/(k_B T_E)]\}$ with an effective electron temperature T_E , where the chemical potential μ is determined by $\sum_{N=0}^4 f_N = \nu/2 = 1.25$. The $N+1\rightarrow N$ transition contributes $(N+1)\{f_{N+1}(1-f_N)\}$ to the CE intensity, where the prefactor $(N+1)$ takes account of the matrix element for the dipole transition between Harmonic oscillator functions.

The experimental spectra for $I=50$ and $300 \mu\text{A}$ are replotted, respectively, in the upper and the lower panels of Figs. 4(a) and 4(b). In the upper panel ($I=50 \mu\text{A}$), the black solid line represents a theoretical line assuming $T_E=25 \text{ K}$ and gives a reasonable fit to the experimental spectra of both the source and drain hot spots. Thin black lines represent respective contributions of $N+1\rightarrow N$ transitions ($N=0-3$), each of which is taken to be a Lorentzian line with $\Gamma=4.35 \text{ cm}^{-1}$ and the resonance frequency, ω_N , shifted at a

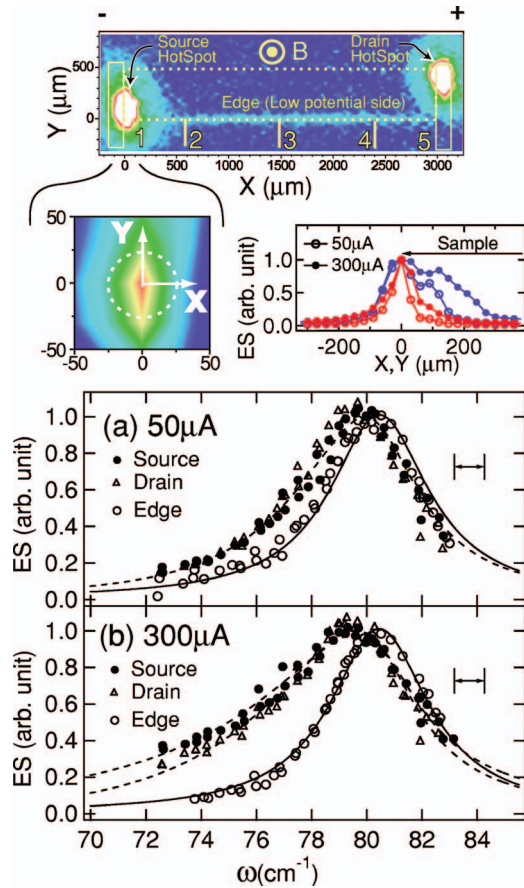


FIG. 2. (Color) Top panel: a CE image at $B=6.02$ T and $I=50$ μA . Broken lines show the outline of the Hall bars studied. Shown below are a blowup of the image with a dotted circle giving a measure of the microscope resolution, and the intensity profiles (red and blue lines, respectively, along the X and the Y directions) about the source hot spot. (a) and (b) Emission spectra at $I=50$ and 300 μA . The solid lines in (a) and (b) are a Lorentzian curve (see the text), while dotted lines are guides for eyes. A bar marks the spectral resolution.

step of -1.9% . The transitions of $N=0$ and 1 dominate while those of $N=2$ and 3 are negligible.

The lower panel ($I=300$ μA) shows that theoretical lines assuming a single electron temperature, $T_E=30$ K (black lines), 100 K (green lines), or 300 K (blue lines), fail to reproduce experimental spectra. The difficulty is that a remarkably high $T_E(>100$ K) is requisite for the account of lower frequency components but it inevitably gives rise to a significant peak shift that is not observed. We interpret this as a consequence that the finite area under study, determined by the spatial resolution of the microscope (50 μm), cannot be characterized by a single value of T_E . Right at the injection point of source hot spot, T_E may be very high ($T_E \geq \hbar\omega_c/k_B=120$ K) since different LLs ($N=0-4$) are fed with electrons more-or-less equally via optical phonon emissions. In the slow cooling-down process that follows, electrons drift away from the point of injection at a speed of E/B . Since the CE primarily takes place during this slow cooling-down process, T_E may decrease as the location moves away from the injection point. The higher- T_E area will

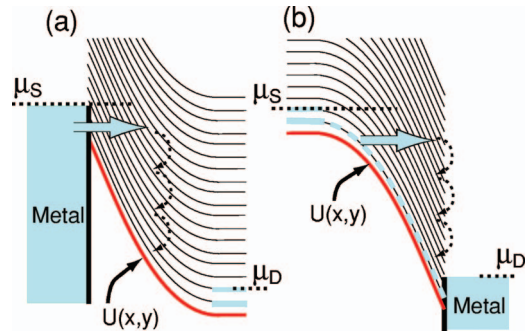


FIG. 3. (Color) Schematic representation of the electron tunneling to higher LLs (fat arrows) followed by cascadelike emissions of optical phonons (dotted round arrows) at the source hot spot (a) and the drain hot spot (b).

progressively expands as I increases because the electrons drift away at higher speeds. Similar discussion may be possible for the drain hot spot as well.

The model in the above may be most simply tested by assuming two different T_E 's. The red dotted lines in the lower panel of Figs. 3(a) and 3(b) represent a theoretical spectrum obtained by superposing the spectra of $T_E=300$ K on the one of $T_E=30$ K at the intensity ratio of $30:70$ ($1:99$ in terms of area). These lines yield much better fit to the experimental spectra. Each contribution from $N+1 \rightarrow N$ transition is elucidated by the thin black lines (30 K) and the red broken lines (300 K). The higher-level transitions ($N=3, 2$) arising from the higher- T_E region (300 K) yield lower-frequency components, while the lower-level transitions ($N=0, 1$) in the lower- T_E region (30 K) primarily determine the peak position. The fitting of the spectra at $I=50$ μA is

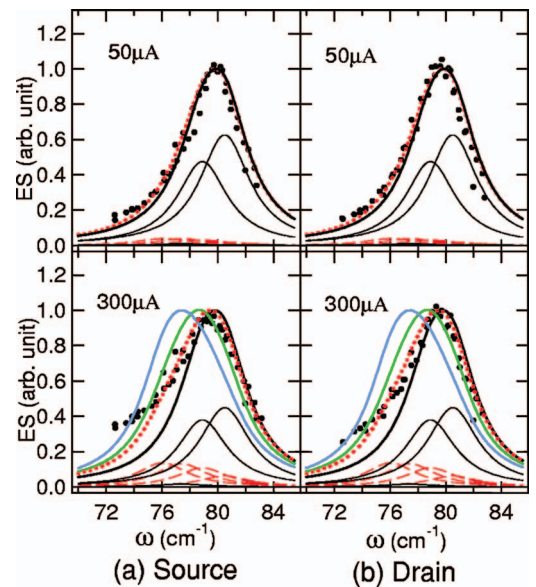


FIG. 4. (Color) Replots of the emission spectra in the source (a) and in the drain (b) hot spots at $I=50$ μA (upper panel) and 300 μA (lower panel). Solid lines represent theoretical spectra at elevated T_E 's; thick black lines in the upper panel ($T_E=25$ K); black (30 K), green (100 K), and blue (300 K) lines in the lower panel. See the text for the other lines.

also improved in the lower frequency region if we add the spectrum of 300 K to that of 25 K with the intensity ratio of 10:90 (0.1:99.9 in terms of area) as shown by the red dotted line in the upper panels of Figs. 4(a) and 4(b). Though not explicit in Fig. 4, the peak emission intensity in this calculation increases by a factor of three from $I=50$ to $300 \mu\text{A}$, which agrees with the experimental finding, giving additional support to the present analysis.

Discrepancy still remains in a lower frequency range for $I=300 \mu\text{A}$; viz., experimental spectra are of larger components. This may be attributed to the simplified assumptions adopted here; (i) the electron distribution is sharply cut off at $N=4$ LL and (ii) the broadening parameter is fixed for different transitions. Though not shown here, much better agreement can be obtained if we assume small contributions from higher LLs ($N=5$ and 6) and increasing values of Γ (by $10\% \sim 25\%$) with increasing N (by 1). Polaron effect may also contribute to shift the CE frequencies towards lower frequencies for higher-level transitions.^{29,30}

If the second derivative, $U''(x)$, of the electrostatic potential with respect to the coordinate x is finite, CE frequency should shift by $\Delta\omega_c = U''(x)l_B^2/(2\hbar)$. The relative shift, $\Delta\omega_c/\omega_c$, is expected to be small in general, since $U(x)$ is smoothed out over the screening length $\lambda \gg l_B$ of the 2DEG. In fact, we find no systematic ω_c shift ascribable to this effect, probably due to the fact that the CE primarily occurs in a region not right at the injection point.

U. Klaß *et al.* studied temperature rise of the hot spots through the fountain-pressure effect of superfluid liquid helium and reported $\Delta T = 10 \mu\text{K}$ ($I=30 \mu\text{A}$, $\nu=2$),⁵ which is by many orders of magnitude smaller than T_E found here. Studied in Ref. 5 is the lattice temperature. The discrepancy may be understood by noting that (i) locally heated lattice spots can be efficiently cooled down by the ballistic passage of acoustical phonons,³¹ whereas the energy relaxation of the electron system relies on the relatively weak electron-phonon interaction and (ii) the heat capacity of the lattice is far larger than the quantized 2DEG system.

In summary, spectra of CE have been studied in quantum Hall bars. The spectra of CE at the current entry and exit corners are remarkably broadened towards lower frequencies with increasing I up to $300 \mu\text{A}$, indicating substantial relevance of nonequilibrium electrons generated in higher-level LLs with N up to 4 ; in terms of effective electron temperature, T_E reaching as high as 300 K is suggested.

This work is supported by the Grant-in-Aid for Specially Promoted Research from Japanese Ministry of Education, Culture, Sports, Science and Technology, and by the Solution Oriented Research for Science and Technology (SORST) from Japan Science and Technology (JST). One of the authors (H.S.) is supported by the Grant-in-Aid for Japan Society for the Promotion of Science (JSPS).

-
- ¹J. Wakabayashi and S. Kawaji, J. Phys. Soc. Jpn. **44**, 1839 (1978).
- ²F. F. Fang and P. J. Stiles, Phys. Rev. B **27**, 6487 (1983); G. L. J. A. Rikken, J. A. M. M. van Haaren, W. van der Wel, A. P. van Gelder, H. van Kempen, P. Wyder, J. P. Andre, K. Ploog, and G. Weimann, *ibid.* **37**, 6181 (1988).
- ³K. von Klitzing, G. Ebert, N. Kleinmichel, and H. Obloh, in *Proceedings of the 17th International Conference on the Physics of Semiconductors*, edited by J. D. Chadi and W. A. Harrison (Springer, New York, 1985), p. 271.
- ⁴P. A. Russell, F. F. Ouali, N. P. Hewett, and L. J. Challis, Surf. Sci. **229**, 54 (1990).
- ⁵U. Klaß, W. Dietsche, K. von Klitzing, and K. Ploog, Z. Phys. B: Condens. Matter **82**, 351 (1991).
- ⁶N. N. Zinov'ev *et al.*, Semicond. Sci. Technol. **9**, 831 (1994).
- ⁷S. Roshko, W. Dietsche, and L. J. Challis, Phys. Rev. Lett. **80**, 3835 (1998).
- ⁸Y. Kawano, Y. Hisanaga, and S. Komiyama, Phys. Rev. B **59**, 12537 (1999).
- ⁹Y. Kawano and S. Komiyama, Phys. Rev. B **61**, 2931 (2000).
- ¹⁰Y. Kawano and S. Komiyama, Phys. Rev. B **68**, 085328 (2003).
- ¹¹B. Jeckelmann and B. Jeanneret, Rep. Prog. Phys. **64**, 1603 (2001).
- ¹²S. Kawaji, K. Hirakawa, M. Nagata, T. Okamoto, T. Fukuse, and T. Gotohet, J. Phys. Soc. Jpn. **63**, 2303 (1994).
- ¹³M. Buttiker, Phys. Rev. Lett. **57**, 1761 (1986); Phys. Rev. B **38**, 9375 (1988).
- ¹⁴S. Komiyama and H. Hirai, Phys. Rev. B **40**, 7767 (1989).
- ¹⁵P. C. van Son, G. H. Kruithof, and T. M. Klapwijk, Phys. Rev. B **42**, 11267 (1990).
- ¹⁶Y. Kawano and S. Komiyama, *Recent Research Developments in Physics 3* (Transworld Research Network, Lerala, India, 2002), p. 129.
- ¹⁷F. Thiele, U. Merkt, J. P. Kotthaus, G. Lommer, F. Malcher, U. Rossler, and G. Weimann, Solid State Commun. **62**, 841 (1987).
- ¹⁸W. Zawadzki, C. Chaubet, D. Dur, W. Knap, and A. Raymond, Semicond. Sci. Technol. **9**, 320 (1994).
- ¹⁹K. Ikushima, H. Sakuma, and S. Komiyama, Rev. Sci. Instrum. **74**, 4209 (2003).
- ²⁰H. Sakuma, K. Ikushima, S. Komiyama, and K. Hirakawa (unpublished).
- ²¹K. Ikushima, H. Sakuma, S. Komiyama, and K. Hirakawa, Phys. Rev. Lett. **93**, 146804 (2004).
- ²²K. Hirakawa, K. Yamanaka, M. Endo, M. Saeki, and S. Komiyama, Phys. Rev. B **63**, 085320 (2001).
- ²³A. Lorke, J. P. Kotthaus, J. H. English, and A. C. Gossard, Phys. Rev. B **53**, 1054 (1996).
- ²⁴The electric field in the vicinity of hot spots, $E_{HS} \approx V_{SD}/\lambda > 1 \times 10^7$ V/m (λ ; the effective screening length assumed to be about 100 nm), largely exceeds $\hbar\omega_c/(el_B) \approx 1 \times 10^6$ V/m, where $l_B = (\hbar/eB)^{1/2} \approx 10$ nm is the magnetic length. Different LLs are, hence, expected to be strongly tunnel coupled.
- ²⁵P. Hawker, A. J. Kent, O. H. Hughes, and L. J. Challis, Semicond. Sci. Technol. **7**, B29 (1992).

- ²⁶Though the magnetophonon-resonance condition, $E_M - E_N = \hbar \omega_{op}$, is not strictly fulfilled for each level, the rate of optical phonon emission may be much higher in the higher energy range of $E > E_1 + \hbar \omega_{op}$.
- ²⁷U. Rossler, *Solid State Commun.* **49**, 943 (1984).
- ²⁸Equation (1) is derived by solving simultaneous Eqs. (6) and (7) in Ref. 18 in the limit of $E_N \ll E_g^*$.
- ²⁹G. Lindemann, R. Lassnig, W. Seidenbusch, and E. Gornik, *Phys. Rev. B* **28**, 4693 (1983).
- ³⁰E. Batke, K. Bollweg, U. Merkt, C. M. Hu, K. Kohler, and P. Ganser, *Phys. Rev. B* **48**, 8761 (1993).
- ³¹K. R. Strickland, R. E. George, M. Henini, and A. J. Kent, *Semicond. Sci. Technol.* **9**, 786 (1994).